Research Article Vol. 34, No. 9 / 4 May 2026 / Optics Express 15979
Optics EXPRESS

Projector radiometric compensation using a 2D spectroradiometer

YOSHIAKI MAEDA* AND DAISUKE IWAI

Graduate School of Engineering Science, The University of Osaka, Osaka 565-0871, Japan
maeda.yoshiaki.286@ecs.osaka-u.ac.jp

Abstract: Projection mapping (PM) optically overlays computer-generated imagery onto real-world objects, enabling users to experience augmented reality without wearing any display devices. However, surface textures often cause color distortion, leading the displayed colors to deviate from the desired colors. To address this issue, we propose a projector radiometric compensation method that minimizes the color difference between a target image and the projected result using a 2D spectroradiometer (2DSR). In the proposed method, we model the color transformation between the projector and the 2DSR in a differentiable manner. Based on this formulation, we propose two optimization strategies for projector radiometric compensation: (i) minimizing the spectral error between the target appearance and the projected result, and (ii) minimizing the color difference measured in a differentiable color space designed to reflect human visual perception. Experiments with a physical prototype demonstrate that our method achieves more accurate projector radiometric compensation and better alignment with human color perception than conventional methods using an RGB camera.

1. Introduction

Projection mapping (PM) is a technique that modulates the color and texture of an object by projecting computer-generated images onto a target object in the real world. Because it can present visual content without requiring users to wear special equipment, PM has been applied not only to entertainment [1–3] but also to various fields such as medical applications [4], makeup [5,6], design support [7–9], and object search tasks [10–13]. However, in most cases, real-world objects have inherent colors and patterns and exhibit non-ideal surface reflectance properties for projection. As a result, color distortion occurs in the projected appearance, and the desired colors cannot be reproduced.

To minimize the impact of residual color distortion in the projected results, various projector radiometric (photometric) compensation methods have been proposed. These methods estimate compensated projector inputs by solving the inverse of a forward color transformation model that maps RGB pixel values input to a projector to RGB pixel values obtained by capturing the projection results with a camera, thereby reproducing the target colors. Nayar et al. [14] approximated the color transformation with a linear model and introduced a 3×3 color transformation matrix. Yoshida et al. [15] improved this approach by adding a term that accounts for ambient light and introduced a 3×4 color transformation matrix. However, because projectors exhibit device-specific nonlinear components in their color processing, simple linear models do not provide sufficient compensation accuracy. To address this, Grundhöfer et al. [16] proposed a method based on thin plate splines to handle the projector nonlinearity, and further achieved projector radiometric compensation that is robust to clipping errors and misalignment in the projector-camera (ProCam) system. In recent years, many methods using deep learning for projector radiometric compensation have also been proposed [17–20]. With deep learning, complex device-specific nonlinearities can be handled, enabling more accurate projector radiometric compensation. End-to-end methods that simultaneously perform geometric

#596052 https://doi.org/10.1364/OE.596052
Journal © 2026 Received 18 Feb 2026; revised 8 Apr 2026; accepted 8 Apr 2026; published 20 Apr 2026

Optics EXPRESS

correction and blur compensation in the ProCam system, in addition to radiometric compensation, have also been proposed [21–23].

However, conventional projector radiometric compensation methods minimize color differences in the color space of images captured by an RGB camera, i.e., within a camera-specific color space, and do not sufficiently consider differences from the colors perceived by humans. It is known that even with camera color calibration [24], the perceived color for a human observer and the captured color cannot, in general, be made identical [25]. This is because the Luther–Ives condition [26,27], which requires that the camera spectral sensitivities be representable as a linear combination of the CIE XYZ color-matching functions, is not satisfied in practice. Therefore, even if radiometric compensation makes the projected result perfectly match the desired colors in the RGB camera image, a human observer viewing the projection directly may still perceive color distortion. A related line of research has explored color appearance modulation using spatially variable laser illumination. In particular, Zhang et al. [28] used programmable laser-based illumination together with spectral measurements to tune the color appearance of illuminated objects by minimizing perceptual color differences. Although this study is related in its use of spectral information and projection-based illumination hardware, its goal is different from projector radiometric compensation. Their focus is on optimizing illumination for color appearance enhancement, whereas our focus is on reproducing a desired projected image on projection surfaces with non-ideal surface colors and textures by compensating for surface-dependent color distortion.

In this paper, we propose a method that overcomes the fundamental limitation of projector radiometric compensation caused by RGB cameras by introducing a 2D spectroradiometer (2DSR), which captures pixel-wise spectral radiance data of the projected result instead of RGB images. We develop a technique that performs color compensation in the spectral radiance domain rather than in a device-dependent RGB color space, by proposing a color transformation model that represents the relationship between RGB input values to the projector and the visible-light spectral data captured by the 2DSR (401 spectral bands in this study). Using this model, we optimize the projector input RGB values to reduce spectral discrepancies from the target appearance, thereby lowering the risk of observer metameric failure. Nevertheless, due to metamerism, reducing spectral error does not guarantee a corresponding reduction in perceptual (or colorimetric) error. To address this issue, we further propose projector radiometric compensation methods that account for human color perception by defining objective functions in perceptually motivated color spaces. In particular, we formulate separate objective functions that minimize errors either in a perceptually motivated RGB color space or in the CIE LAB color space [29], with differentiable conversions from spectral data to these spaces.

The main contributions of this study are as follows.

- To the best of our knowledge, we propose the first projector radiometric compensation framework that uses a 2DSR to model pixel-wise spectral radiance of projected results.
- We formulate projector radiometric compensation as an optimization problem in the spectral radiance domain, and further introduce perceptually motivated objectives through differentiable conversions from spectral data to perceptual color spaces.
- Experiments with a physical prototype demonstrate that the proposed method achieves more accurate and perceptually consistent compensation than conventional RGB-camera-based methods.

2. Method

The 2DSR captures, on a per-pixel basis, the spectral distribution of light reflected from the projection surface under projector illumination. To realize pixel-wise projector radiometric

Optics EXPRESS

compensation, we obtain pixel correspondences between the 2DSR and the projector using the Gray-code pattern projection method [30]. In the following, we first summarize prerequisites, including the conversion between per-pixel spectral representations and RGB pixel values, and then describe the modeling of the projector-2DSR system and the estimation of its model parameters. Next, we explain the optimization objective functions and their gradients for radiometric compensation, and finally summarize the procedures for estimation and projection-image update as algorithms.

2.1. Prerequisites

Since this study uses an RGB projector, spectral images must be converted into RGB images before projection. To map spectral data to an RGB color space, we first convert it to the XYZ color space using the CIE 1931 standard observer color-matching functions [31], and then linearly project it into an arbitrary RGB color space. In this study, we adopted the CIE 1931 2° Standard Observer because the projection target used in our experiments was a relatively small object (approximately 200 mm × 200 mm), and the assumed viewing distance was approximately 900 mm. The color-matching functions are denoted as $\bar{x}(\lambda)$, $\bar{y}(\lambda)$, and $\bar{z}(\lambda)$ with respect to wavelength λ. Let a discretized spectral distribution be $S(\lambda) \in \mathbb{R}^{\lambda}$ and $k \in \mathbb{R}$ be a normalization constant. The tristimulus values (X, Y, Z) are then computed as follows and normalized to $[0, 1]$ [29].

$$X = k \sum_{\lambda} S(\lambda)\bar{x}(\lambda)\Delta\lambda, \quad Y = k \sum_{\lambda} S(\lambda)\bar{y}(\lambda)\Delta\lambda, \quad Z = k \sum_{\lambda} S(\lambda)\bar{z}(\lambda)\Delta\lambda. \tag{1}$$

Here, $\Delta\lambda \in \mathbb{R}_+$ denotes the spectral sampling interval. Equation (1) can be written in matrix form as

$$(X, Y, Z)^{\top} = MS. \tag{2}$$

Here, the color-matching matrix $M \in \mathbb{R}^{3\times\lambda}$ represents the color-matching functions (with scaling) in matrix form, and $S \in \mathbb{R}^{\lambda}$ is the vectorized spectral distribution $S(\lambda)$.

To convert tristimulus values (X, Y, Z) into RGB values $(r, g, b \in \mathbb{R})$, we apply a linear projection. Hereafter, we assume that the RGB color space is the sRGB color space (Rec. 709) [32] or a linear color space with the same white point D_{65}. If the RGB values fall outside $[0, 1]$, we apply clipping. Then, if necessary, gamma correction is applied to the obtained RGB values (r, g, b).

2.2. Projector-2DSR color transformation model

Each RGB channel of the projector has its own spectral power distribution. The radiance of each projected pixel follows an inverse-square law with respect to the distance between the projector and the projection surface, and is additionally modulated by the cosine of the incident angle. We refer to this combined attenuation term as the form factor. The spectral radiance of the projected result is modeled as the product of the attenuated spectral power distribution of the projector and the spectral reflectance of the projection surface. Furthermore, environmental light also contributes to the captured spectral data. Taking these factors into account, we model the relationship between an RGB input to the projector and the spectral data of the projected result captured by the 2DSR.

For a projected pixel, let the projector input RGB values be $\mathbf{x}_{\mathrm{rgb}} = (r, g, b)^{\top}$, the spectral power distribution of each primary be $P_m(\lambda) \in \mathbb{R}^{\lambda}$, $m \in \{r, g, b\}$, the spectral reflectance of the projection surface be $\rho(\lambda) \in \mathbb{R}^{\lambda}$, the form factor be $F(\lambda) \in \mathbb{R}^{\lambda}$, and the spectral power distribution of environmental illumination be $E(\lambda) \in \mathbb{R}^{\lambda}$. Here, $E(\lambda)$ is defined for each projected pixel and can therefore vary spatially across the scene. Then, the spectral data of the projected result

Optics EXPRESS

captured at the corresponding 2DSR pixel, $C(\lambda) \in \mathbb{R}_+^{\lambda}$, is expressed as

$$C(\lambda) = \rho(\lambda)F(\lambda)\sum_m P_m(\lambda)x_m + E(\lambda). \tag{3}$$

Since the 2DSR captures discretized spectral data, the vectorized spectral data of the projected result, $\mathbf{C} \in \mathbb{R}_+^{\lambda}$, can be written as the following matrix product:

$$\mathbf{C} = RFP\mathbf{x}_{\text{rgb}} + \mathbf{E} = W\mathbf{x}_{\text{rgb}} + \mathbf{E}. \tag{4}$$

Here, $R \in \mathbb{R}^{\lambda\times\lambda}$ is the spectral reflectance matrix of the projection surface, $F \in \mathbb{R}^{\lambda\times\lambda}$ is the form-factor (diagonal) matrix, $P \in \mathbb{R}^{\lambda\times 3}$ denotes the projector spectral characteristic matrix, whose columns represent the spectral power distributions of the three projector primaries. $\mathbf{E} \in \mathbb{R}^{\lambda}$ denotes the pixel-wise spectral power distribution of environmental illumination. Assuming that the projection system and experimental setup remain fixed, we simplify the product RFP as a constant color transformation matrix $W \in \mathbb{R}^{\lambda\times 3}$. Here, we assume that the projector input $\mathbf{x}_{\text{rgb}}$ is represented in a linear radiometric space. In practice, before model estimation and iterative compensation, we cancel the projector's gamma characteristic by applying the inverse of the calibrated projector gamma function. Specifically, the linearized projector input is given by

$$\mathbf{x}_{\text{rgb}}^{\text{lin}} = \gamma^{-1}(\mathbf{x}_{\text{rgb}}), \tag{5}$$

where $\gamma(\cdot)$ denotes the calibrated projector gamma function applied channel-wise. Under this pre-linearized setting, Eq. (4) is used as a linear approximation of the relationship between projector input and captured spectral radiance.

In our method, we control the projector input RGB values $\mathbf{x}_{\text{rgb}}$ so that the captured spectral data $\mathbf{C}$ approaches a target spectral distribution $\mathbf{T}$. To obtain such projection RGB values using gradient-based optimization, we make the projector-2DSR color transformation differentiable in the spectral radiance domain. To this end, we introduce an auxiliary spectral variable $\mathbf{x}_{\text{spe}} \in \mathbb{R}^{\lambda}$ and express the projector input as $\mathbf{x}_{\text{rgb}} = M_{\text{rgb}}\mathbf{x}_{\text{spe}}$ using the spectrum-to-RGB conversion matrix M_{rgb}, which is a known transformation matrix defined for each RGB color space. Substituting this into Eq. (4), we rewrite the model in the 2DSR spectral space as:

$$\mathbf{C} = WM_{\text{rgb}}\mathbf{x}_{\text{spe}} + \mathbf{E} = G\mathbf{x}_{\text{spe}} + \mathbf{E}, \tag{6}$$

where we define the projection system function $G \in \mathbb{R}^{\lambda\times\lambda}$ as the product WM_{rgb}. Accordingly, for each projected pixel, our problem is to determine the projector input that minimizes a chosen discrepancy between a target spectral distribution and the captured spectral data. Using Eq. (6), this per-pixel optimization problem can be generally written as:

$$\mathbf{x}_{\text{spe}}^{*} = \arg\min_{\mathbf{x}_{\text{spe}}} O\big(\mathbf{T},\ G\mathbf{x}_{\text{spe}} + \mathbf{E}\big), \tag{7}$$

where $O(\cdot)$ denotes a chosen merit function. In the following, we consider merit functions defined on spectral radiance as well as on color spaces derived from spectral radiance.

2.3. Parameter estimation

To estimate the parameters (W and $\mathbf{E}$) of our color transformation model in Eq. (4), we input known RGB values $\mathbf{x}_{\text{rgb}}^{i}$ to the projector and capture the corresponding spectral data $\mathbf{C}^{i}$ using the 2DSR. Since the model is defined per pixel, both W and $\mathbf{E}$ are estimated independently for each

Optics EXPRESS

pixel. W can be estimated by solving the following least-squares problem:

$$\underset{W}{\operatorname{argmin}} \sum_{i=1}^{N} \|\mathbf{C}^i - (W\mathbf{x}^i_{\mathrm{rgb}} + \mathbf{E})\|_2^2. \tag{8}$$

Here, N denotes the number of pairs of captured spectral data and the input RGB values. Let $\tilde{W} = (W \quad \mathbf{E})$ and $\tilde{\mathbf{x}}^i_{\mathrm{rgb}} = (\mathbf{x}^i_{\mathrm{rgb}}; 1)$; then Eq. (8) can be rewritten as:

$$\underset{\tilde{W}}{\operatorname{argmin}} \sum_{i=1}^{N} \|\mathbf{C}^i - \tilde{W}\tilde{\mathbf{x}}^i_{\mathrm{rgb}}\|_2^2. \tag{9}$$

The solution to this least-squares problem is obtained analytically (see Algorithm 1).

In our experiments using a prototype, we input spatially uniform images with at least four different RGB values (i.e., $N = 4$) to the projector, capture the corresponding spectral data using the 2DSR, and estimate W and $\mathbf{E}$.

2.4. Spectral radiometric compensation

To realize radiometric compensation using the 2DSR and the projector, we define objective functions and compute projection colors via gradient-based optimization. We first introduce an objective function that minimizes spectral error. Unlike direct feedback optimization operating in RGB space, our formulation explicitly models the projector–2DSR color transformation in the spectral radiance domain. Therefore, the chosen merit function is not restricted to discrepancies evaluated in RGB space, but can also be defined on spectral radiance or on color spaces derived from spectral radiance. Although the above model is linearized after canceling the projector's gamma characteristic, some residual mismatch may still remain because the actual projector response can include more complex nonlinear effects. Nevertheless, our compensation procedure is iterative and re-captures the actual projected spectrum at each iteration. Therefore, the update is repeatedly based on the measured discrepancy between the target and the current projection result, which provides practical robustness to moderate mismatch between the linear model and the true projector response. However, because the dimensionality of the projection colors is much smaller than that of the captured spectral data, the solution becomes underdetermined, and it is difficult to perfectly reproduce the desired spectral distribution. When spectral error remains, the desired color and the perceived color may not be metamers, and an observer may perceive color distortion. Therefore, in this section, we further consider strategies to minimize color distortion by making the target color and the perceived color metameric, leveraging established knowledge in color science. We introduce two types of objective functions: one that minimizes color differences in linear RGB color spaces, each distinguished by their particular set of primary colors, and another that minimizes color differences in non-linear color spaces such as CIE LAB that reflect perceptual non-uniformity. To enable gradient-based optimization, all three objective functions are designed to be differentiable.

Minimization of spectral error We optimize an auxiliary spectral variable $\mathbf{x}_{\mathrm{spe}}$ such that the spectral data captured by the 2DSR matches the target spectral data $\mathbf{T} \in \mathbb{R}^{\lambda}$. The resulting projector input is obtained as RGB values through the linear mapping $\mathbf{x}_{\mathrm{rgb}} = M_{\mathrm{rgb}}\mathbf{x}_{\mathrm{spe}}$. The per-pixel objective function is defined as follows:

$$O_{\mathrm{spe}}(\mathbf{x}_{\mathrm{spe}}) = \frac{1}{2}\|\mathbf{T} - \mathbf{C}\|_2^2 = \frac{1}{2}\|\mathbf{T} - (G\mathbf{x}_{\mathrm{spe}} + \mathbf{E})\|_2^2. \tag{10}$$

Accordingly, the gradient of the objective function is computed as

$$\nabla O_{\mathrm{spe}}(\mathbf{x}_{\mathrm{spe}}) = -G^{\top}(\mathbf{T} - (G\mathbf{x}_{\mathrm{spe}} + \mathbf{E})). \tag{11}$$

Minimization of error in linear color spaces Equation (10) minimizes the squared error in a spectral domain; however, as described at the beginning of this section, if spectral error remains,

Optics EXPRESS

the target color and the color perceived by the user may not coincide. Thus, we compensate so that the target color and the perceived color become metamers by minimizing the error in a color space based on knowledge of human color perception. Here, we define the spectral error $\mathbf{D} \in \mathbb{R}^{\lambda}$ as the difference between the target and the captured spectral distribution:

$$\mathbf{D} = \mathbf{T} - (G\mathbf{x}_{\text{spe}} + \mathbf{E}). \tag{12}$$

We project this spectral error into an RGB vector $\mathbf{d} \in \mathbb{R}^3$ using the spectrum-to-RGB conversion described in Sec. 2.1. Using a color-matching matrix M that linearly maps spectral distributions to RGB values

$$\mathbf{d} = M\mathbf{D}. \tag{13}$$

When accounting for human color perception, it is preferable to use a color space defined by a transformation matrix M (i.e., color-matching functions) based on the standard observer, such as M_{rgb}. Nevertheless, other color-matching functions can be used as well, including those for linear lightness-separated color spaces or those derived from non-human primate color spaces. To minimize the color difference in the linear color space, we define the objective function as

$$O_{\text{rgb}}(\mathbf{x}_{\text{spe}}) = \frac{1}{2}\|\mathbf{d}\|_2^2. \tag{14}$$

From Eqs. (12) and (13), Eq. (14) is differentiable with respect to $\mathbf{x}_{\text{spe}}$, and its gradient is computed as

$$\begin{aligned} \nabla O_{\text{rgb}}(\mathbf{x}_{\text{spe}}) &= -G^\top M^\top M\mathbf{D} \\ &= -G^\top M^\top M\{\mathbf{T} - (G\mathbf{x}_{\text{spe}} + \mathbf{E})\}. \end{aligned} \tag{15}$$

Minimization of error in non-linear color spaces Minimizing error in a linear color space can compensate so that the target and perceived colors become metamers, but it cannot account for the nonlinearity of human color perception. To compute the projection image in a color space that is approximately perceptually uniform, we minimize the color difference ΔE_{76} in the non-linear CIE LAB color space [29]. We introduce spectral-level differentiation of ΔE_{76} by extending the method of Kauvar et al. [33]. The conversion $\eta : \mathbb{R}_+^3 \to \mathbb{R}^3$ from CIE XYZ to CIE LAB is defined as

$$\begin{aligned} L^* &= 116\phi(Y/W_{\text{y}}) - 16 \\ a^* &= 500\{\phi(X/W_{\text{x}}) - \phi(Y/W_{\text{y}})\} \\ b^* &= 200\{\phi(Y/W_{\text{y}}) - \phi(Z/W_{\text{z}})\} \end{aligned} \tag{16}$$

where $\phi : \mathbb{R}_+ \to \mathbb{R}_+$ is defined as

$$\phi(x) = \begin{cases} x^{\frac{1}{3}} & \text{if } x > \left(\frac{6}{29}\right)^3 \\ \frac{1}{3}\left(\frac{29}{6}\right)^2 x + \frac{4}{29} & \text{otherwise} \end{cases} \tag{17}$$

and $W_{\text{x}}, W_{\text{y}}, W_{\text{z}}$ are the tristimulus values of the white point. For the D_{65} white point, we use $W_{\text{x}} = 0.9505$, $W_{\text{y}} = 1.0000$, and $W_{\text{z}} = 1.0884$. Next, we define the objective function as

$$O_{\text{lab}}(\mathbf{x}_{\text{spe}}) = \frac{1}{2}\|\mathbf{e}_{76}\|_2^2 = \frac{1}{2}(\Delta E_{76})^2. \tag{18}$$

Here, $\mathbf{e}_{76} = (\Delta L^*, \Delta a^*, \Delta b^*)^\top$ is the color-difference vector in the CIE LAB space, and to make it differentiable with respect to $\mathbf{x}_{\text{spe}}$, we define $\mathbf{e}_{76}$ as

$$\mathbf{e}_{76} = \eta(M_{\text{xyz}}\mathbf{T}) - \eta(M_{\text{xyz}}(G\mathbf{x}_{\text{spe}} + \mathbf{E})). \tag{19}$$

Optics EXPRESS

The gradient of the objective function is computed as

$$\begin{aligned}\nabla O_{\mathrm{lab}}(\mathbf{x}_{\mathrm{spe}}) &= -G^{\top} M_{\mathrm{xyz}}^{\top}\{J_{\eta}(M_{\mathrm{xyz}}(G\mathbf{x}_{\mathrm{spe}}+\mathbf{E}))\}^{\top}\mathbf{e}_{76} \\ &= -G^{\top} M_{\mathrm{xyz}}^{\top}\{J_{\eta}(M_{\mathrm{xyz}}(G\mathbf{x}_{\mathrm{spe}}+\mathbf{E}))\}^{\top}\{\eta(M_{\mathrm{xyz}}\mathbf{T}) - \eta(M_{\mathrm{xyz}}(G\mathbf{x}_{\mathrm{spe}}+\mathbf{E}))\}.\end{aligned} \tag{20}$$

Here, M_{xyz} denotes the transformation matrix from spectral data to the CIE XYZ color space, and $J_{\eta} \in \mathbb{R}^{3\times 3}$ denotes the Jacobian matrix defined as

$$J_{\eta} = \begin{bmatrix} 0 & 116\phi'(Y, W_{\mathrm{y}}) & 0 \\ 500\phi'(X, W_{\mathrm{x}}) & -500\phi'(Y, W_{\mathrm{y}}) & 0 \\ 0 & 200\phi'(Y, W_{\mathrm{y}}) & -200\phi'(Z, W_{\mathrm{z}}) \end{bmatrix}. \tag{21}$$

Here, $\phi'(x, w)$ denotes the derivative of Eq. (17), defined as

$$\phi'(x, w) = \begin{cases} \frac{1}{3w^{1/3}} x^{-\frac{2}{3}} & \text{if } \frac{x}{w} > \left(\frac{6}{29}\right)^3 \\ \frac{1}{3w}\left(\frac{29}{6}\right)^2 & \text{otherwise} \end{cases} \tag{22}$$

2.5. Updating projection image

In this section, we mathematically described the estimation of the parameters of our projector–2DSR color transformation model and the computation used to update the projection image. However, in practical implementation, gamma correction and conversions from spectral data to RGB values must be applied at appropriate stages of the pipeline, which requires careful handling. In this study, we estimate the model parameters and update the projection image following the procedures described in Algorithm 1 and Algorithm 2, respectively.

Algorithm 1. Estimation of projection function *W*

Input: Set of known RGB values $\{\mathbf{x}_{\mathrm{rgb}(i)}\}_{i=1}^{N}$ $(N \geq 4)$, gamma correction function $\gamma^{-1}(\cdot)$
Output: Estimated projection function $\hat{W} \in \mathbb{R}^{\lambda\times 3}$ and disturbance spectrum $\hat{\mathbf{E}} \in \mathbb{R}^{\lambda}$

for $i = 1$ to N **do** ▷ Gamma correction
  $\mathbf{x}'_{\mathrm{rgb}(i)} \leftarrow \gamma^{-1}(\mathbf{x}_{\mathrm{rgb}(i)})$
end for
for $i = 1$ to N **do** ▷ Capture spectra
  Project uniform image with $\mathbf{x}'_{\mathrm{rgb}(i)}$
  Capture $\mathbf{C}_{(i)} \in \mathbb{R}^{\lambda}$ using 2DSR
end for
for $i = 1$ to N **do** ▷ Augment RGB vectors
  $\tilde{\mathbf{x}}_{\mathrm{rgb}(i)} \leftarrow (\mathbf{x}_{\mathrm{rgb}(i)}^{\top}, 1)^{\top}$
end for
$\tilde{X} \leftarrow (\tilde{\mathbf{x}}_{\mathrm{rgb}(1)}, \ldots, \tilde{\mathbf{x}}_{\mathrm{rgb}(N)})$ ▷ $\in \mathbb{R}^{4\times N}$
$C \leftarrow (\mathbf{C}_{(1)}, \ldots, \mathbf{C}_{(N)})$ ▷ $\in \mathbb{R}^{\lambda\times N}$
$\hat{\tilde{W}} \leftarrow C\tilde{X}^{\dagger}$ ▷ Least squares (Moore–Penrose) solution
$\hat{W} \leftarrow \hat{\tilde{W}}_{[:,1:3]}$ ▷ Extract first 3 columns
$\hat{\mathbf{E}} \leftarrow \hat{\tilde{W}}_{[:,4]}$ ▷ Extract last column
return $\hat{W}$ and $\hat{\mathbf{E}}$

Optics EXPRESS

Algorithm 2. Spectral radiometric compensation with iterative optimization

Input: Target spectrum $\mathbf{T} \in \mathbb{R}^{\lambda}$, Objective function $O(\cdot)$, Initial projection spectrum $\mathbf{x}_{\text{spe}}^{(0)}$, gamma correction $\gamma^{-1}(\cdot)$, projection function $W \in \mathbb{R}^{\lambda \times 3}$, spectrum-to-RGB matrix $M_{\text{rgb}} \in \mathbb{R}^{3 \times \lambda}$, spectrum-to-XYZ matrix $M_{\text{xyz}} \in \mathbb{R}^{3 \times \lambda}$, Lab function $\eta(\cdot) : \mathbb{R}^3 \to \mathbb{R}^3$
Output: Optimized projection image $\mathbf{x}_{\text{spe}}^{*} \in \mathbb{R}^{\lambda}$

if $\mathbf{x}_{\text{spe}}^{(0)}$ is given **then**
  $\mathbf{x}_{\text{spe}} \leftarrow \mathbf{x}_{\text{spe}}^{(0)}$ ▷ Initialize with given spectrum
else
  $\mathbf{x}_{\text{spe}} \leftarrow \mathbf{T}$ ▷ Initialize with target
end if
$\mathbf{e}_{76} \leftarrow \mathbf{0}$ ▷ Initialize Lab error
$G \leftarrow W M_{\text{rgb}}$ ▷ Projection system function
for each iteration **do**
  $\mathbf{x}_{\text{rgb}} \leftarrow \gamma^{-1}(M_{\text{rgb}} \mathbf{x}_{\text{spe}})$ ▷ Spectrum to RGB
  Project $\mathbf{x}_{\text{rgb}}$
  Capture $\mathbf{C} \in \mathbb{R}^{\lambda}$ using 2DSR
  if O_{lab} is used **then**
    $\mathbf{e}_{76} \leftarrow \eta(M_{\text{xyz}} \mathbf{T}) - \eta(M_{\text{xyz}} \mathbf{C})$ ▷ Lab error
  end if
  $\nabla \mathbf{x}_{\text{spe}} \leftarrow$ Gradient calculation$(\mathbf{C}, \mathbf{x}_{\text{spe}}, \mathbf{T}, O, M_{\text{rgb}}, M_{\text{xyz}}, G, \mathbf{e}_{76})$
  $\mathbf{x}_{\text{spe}} \leftarrow$ Optimizer$(\mathbf{x}_{\text{spe}}, \nabla \mathbf{x}_{\text{spe}})$
  if $\mathbf{x}_{\text{spe}}$ is converged **then**
    $\mathbf{x}_{\text{spe}}^{*} \leftarrow \mathbf{x}_{\text{spe}}$
    break
  end if
end for
return $\mathbf{x}_{\text{spe}}^{*}$

3. Experiment

To validate the effectiveness of the proposed method, we conducted projection experiments in a physical environment. We also performed comparative evaluations between the proposed method and two baseline methods implemented using an RGB camera [15,18].

3.1. System configuration and setup

We performed radiometric compensation and projection using a projector (EPSON EB-FH52, resolution: 1920×1080) and a 2DSR (TOPCON SR-5100, effective pixels: 2448×2048). The computer specifications were (CPU: i9-10920X @ 3.50 GHz, GPU: NVIDIA GeForce RTX 3060Ti, RAM: 256 GB). We used L-BFGS [34] as the optimizer and ran optimization for up to 50 iterations. For the baseline methods, we used an RGB camera (Canon M6 Mark2, resolution: 6960×4640).

There is a difference in color reproduction between (i) an RGB image obtained by converting a 2DSR-captured spectral image using CIE 1931 2° color matching functions [31] and (ii) an RGB image captured by the RGB camera, due to differences between the RGB camera spectral sensitivities and the color matching functions. Therefore, we performed color calibration of the RGB camera using a Calibrite ColorChecker Mini based on the method of Finlayson et al. [24].

As the projection surface, we used papers with patterns printed by an inkjet printer. The surface was placed in front of the projector, and the distance between the projector and the surface was set to 0.8 m. The implemented setup is shown in Fig. 1. As the target spectral image, we used spectral images captured by the 2DSR of real planar surfaces while they were illuminated with the projector's white light.

Optics EXPRESS

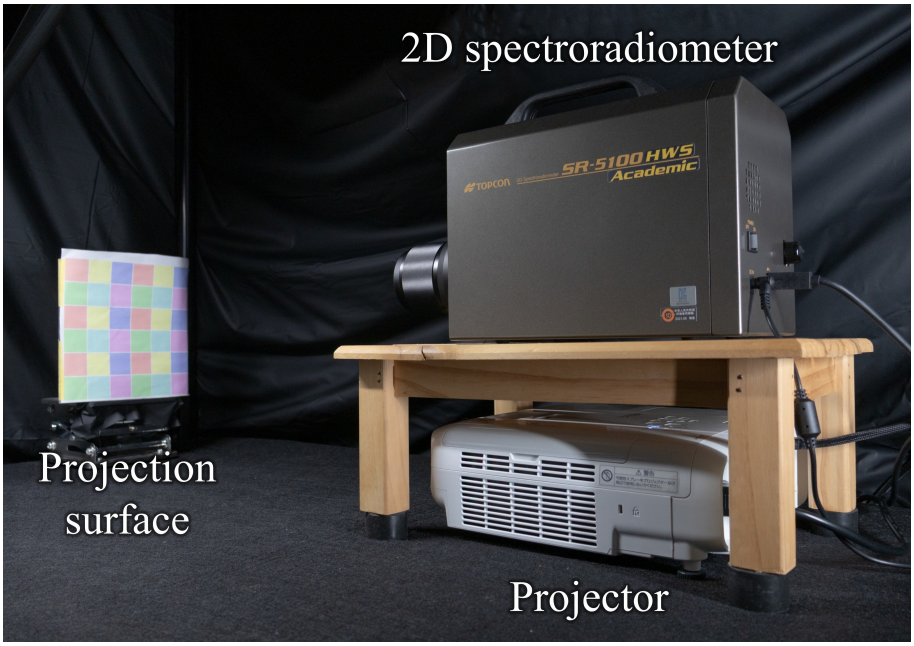

Fig. 1. Experimental setup.

3.2. Ablation study

As described in Sec. 2.4, our method introduces three objective functions: minimization of spectral error, minimization of error in a linear color space, and minimization of error in a non-linear color space. We evaluated and compared the projected results obtained by varying the objective function O used for radiometric compensation. As objective functions, we used O_{spe} for minimizing spectral error, O_{rgb} for minimizing color differences in the sRGB color space, O_{lab} for minimizing color differences in the CIE LAB color space, and all combinations of these objective functions. To make optimization converge faster and more stably, we used the target spectral distribution $\mathbf{T}$ as the initial projection image for O_{spe}, and otherwise used the spectral distribution $\mathbf{x}^*_{\mathrm{spe}}$ which was obtained by optimizing O_{spe}.

Figure 2 shows the projection results obtained with each objective function, and Table 1 reports the quantitative metrics. As evaluation metrics, we used the mean absolute error (MAE) between the target and captured spectral images, the peak signal-to-noise ratio (PSNR) in the sRGB color space, and the mean color difference in the CIE LAB color space (ΔE_{76}, Illuminant D_{65}). PSNR is defined as $\mathrm{PSNR} = 10\log_{10}\left(I^2_{\max}/\mathrm{MSE}\right)$, where $I_{\max}$ is the maximum possible pixel value (higher PSNR indicates smaller error). Here, the suffix "(RGB)" indicates that the metric is computed in the RGB (sRGB) color space. As shown in Table 1, when using O_{spe}, O_{rgb}, and O_{lab} individually, each objective function minimized the error in its corresponding space. In addition, the combination $O_{\mathrm{rgb}} + O_{\mathrm{lab}}$ achieved high accuracy comparable to the results obtained by optimizing each individual objective function, as indicated by PSNR (RGB) and ΔE_{76} in the CIE LAB color space. Furthermore, combining all objective functions, $O_{\mathrm{spe}} + O_{\mathrm{rgb}} + O_{\mathrm{lab}}$, yielded consistently good results across all metrics.

As shown in Fig. 2(a), for all objective functions, color distortion between the target image and the projection result was substantially reduced compared with the case without compensation (w/o comp.). Moreover, as shown in Fig. 2(b), radiometric compensation with the proposed method makes the captured spectral distribution closer in shape to the target spectral distribution.

Optics EXPRESS

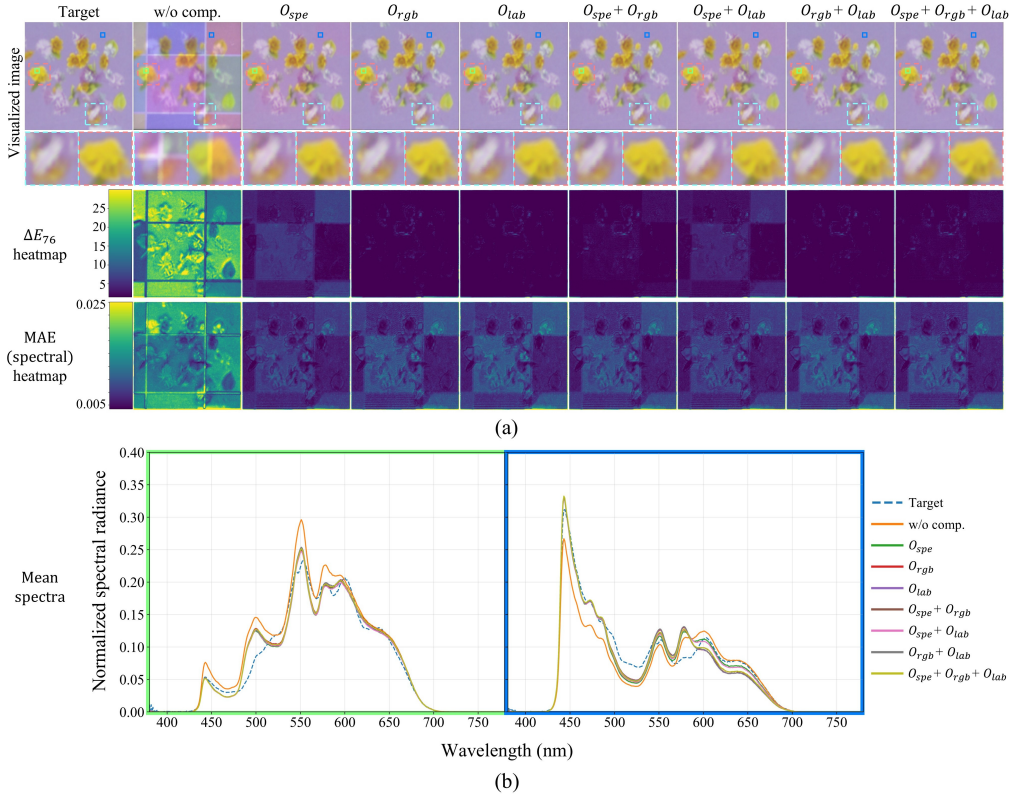

Fig. 2. Comparison of projection results across objective functions. (a) Visualization images obtained by capturing the proposed-method projections with the 2DSR and converting them to the sRGB color space, along with heatmaps of ΔE_{76} between the target spectral image and the projection result and the spectral MAE. The corresponding error heatmaps for each column are shown in the second and third rows. To effectively visualize error changes due to different objective functions, the heatmap ranges are clipped at the 98th percentile of the error values. (b) Comparison of mean spectra within the solid rectangular region indicated in the visualization images.

Table 1. Comparison of quantitative evaluations across projection results.

Method	MAE (Spectral) ($\times 10^{-3}$) (↓)	PSNR (RGB) (↑)	ΔE_{76} (↓)
w/o comp.	14.79	22.0	19.51
O_{spe}	7.31	32.3	4.57
O_{rgb}	8.07	36.7	1.00
O_{lab}	8.36	35.8	0.85
$O_{\mathrm{spe}}+O_{\mathrm{rgb}}$	7.92	36.2	1.82
$O_{\mathrm{spe}}+O_{\mathrm{lab}}$	7.36	33.5	3.44
$O_{\mathrm{rgb}}+O_{\mathrm{lab}}$	8.33	36.7	0.90
$O_{\mathrm{spe}}+O_{\mathrm{rgb}}+O_{\mathrm{lab}}$	7.82	36.2	1.59

Optics EXPRESS

In particular, when using O_{spe}, the shapes of the target and captured spectral distributions become much closer than with the other objective functions. However, as indicated by the heatmaps in Fig. 2(a) and Table 1, when using O_{spe}, small errors remain in the sRGB and CIE LAB color spaces. This is because, as discussed in Sec. 1, when spectral error is non-zero in spectral-minimization projection, the target color and the perceived color may not coincide. Nevertheless, minimizing spectral error makes the target and captured spectral distributions very similar in shape, and thus provides an effective initialization for subsequent optimization. In addition, minimizing spectral error can mitigate the impact of observer metameric mismatch caused by differences in spectral shapes between the target and the projected result. Therefore, combining it with objective functions that minimize error in color spaces accounting for human color perception can potentially enable better radiometric compensation even for observers who deviate from the standard observer assumed by the color matching functions.

Overall, these results show that each objective function effectively minimizes error in its respective color space. They also show that combining objective functions allows errors in multiple color spaces to be minimized in a balanced manner. Based on these results, in the following experiments we use $O_{\mathrm{rgb}} + O_{\mathrm{lab}}$ and $O_{\mathrm{spe}} + O_{\mathrm{rgb}} + O_{\mathrm{lab}}$ as the objective functions of the proposed method. We also evaluated the convergence behavior of the proposed iterative optimization. Figure 3 shows the transition of the evaluation metrics over the iterations. In addition, the computation time for one iteration under our experimental setup was approximately 2 min, including spectral image acquisition with the 2DSR and optimization.

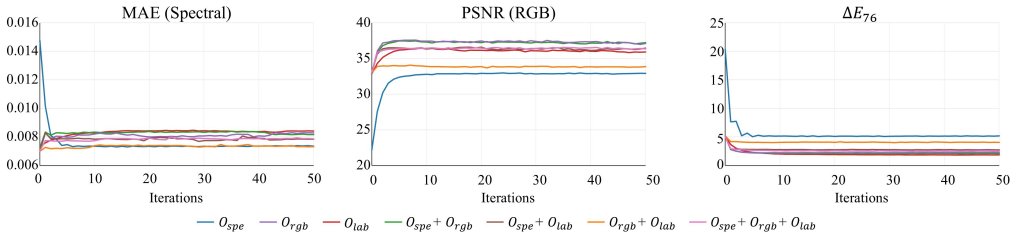

Fig. 3. Convergence behavior of the proposed iterative optimization. The evaluation metrics are plotted as a function of the iteration number.

3.3. Comparison with baseline methods

In this section, we implemented the methods of Yoshida et al. [15] and Huang et al. [18] as baseline methods and compared them with the proposed method. For geometric correction, we used the Gray-code pattern projection method, as in the proposed method. Therefore, as the method of Huang et al. [18], we adopted CompenNest w/SL, which performs only radiometric compensation, and used the training dataset released by Huang et al. for model training. Figure 4 shows the projection results of each method, and Table 2 reports the evaluation metrics.

As shown in Fig. 4(a), compared with projection without compensation, both the method of Yoshida et al. [15] and the method of Huang et al. [18] reduce color distortion between the target image and the projection result. However, the ΔE_{76} and spectral-MAE heatmaps indicate that, for both methods, color distortion between the target image and the projection result remains large. In contrast, the proposed method substantially reduces color distortion between the target image and the projection result. In particular, when using $O_{\mathrm{spe}} + O_{\mathrm{rgb}} + O_{\mathrm{lab}}$, the errors in both heatmaps become small. Moreover, as shown in Fig. 4(b), radiometric compensation with the proposed method makes the captured spectral distribution closer in shape to the target spectral distribution among all methods. As shown in Table 2, for both objective function combinations, the proposed method outperforms the baseline methods on all evaluation metrics. In particular,

Optics EXPRESS

when using $O_{\mathrm{rgb}} + O_{\mathrm{lab}}$, ΔE_{76} achieves the smallest value of 0.86, demonstrating radiometric compensation that better aligns with human color perception.

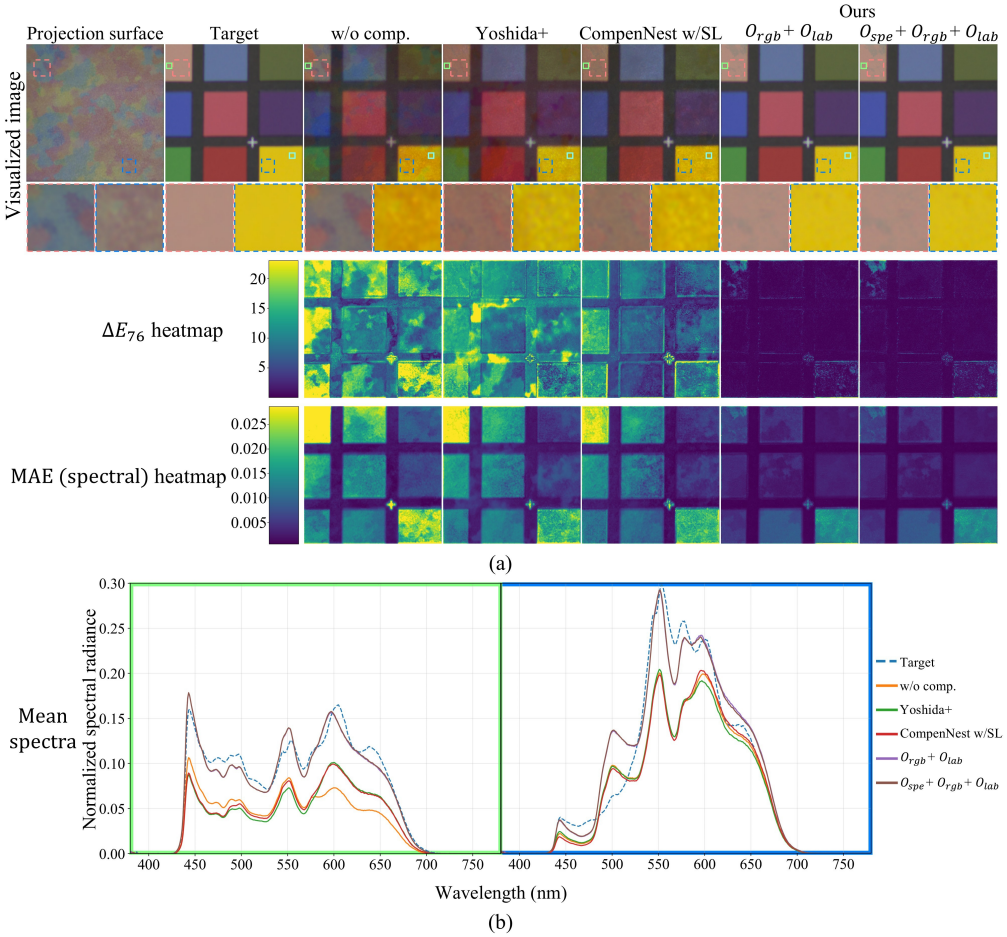

Fig. 4. Comparison of projection results across methods. (a) Visualization images obtained by capturing the proposed-method projections with the 2DSR and converting them to the sRGB color space, along with heatmaps of ΔE_{76} between the target spectral image and the projection result and the spectral MAE. (b) Comparison of mean spectra within the solid rectangular region indicated in the visualization images.

Table 2. Comparison of quantitative evaluation between baseline methods and the proposed method.

Metric	w/o comp.	Yoshida [15]	CompenNeSt w/SL [18]	$O_{\mathrm{rgb}}+O_{\mathrm{lab}}$	$O_{\mathrm{spe}}+O_{\mathrm{rgb}}+O_{\mathrm{lab}}$
MAE (Spectral) ($\times 10^{-3}$) (↓)	11.52	10.39	9.09	4.18	**4.10**
PSNR (RGB) (↑)	21.4	22.8	24.5	39.8	**40.3**
ΔE_{76} (↓)	12.74	12.12	8.09	**0.86**	0.99

4. Discussion and limitations

In this paper, we proposed a projector radiometric compensation method with high color reproduction accuracy using a 2DSR. Most conventional projector radiometric compensation

Optics EXPRESS

methods have been based on image acquisition with an RGB camera. However, RGB camera spectral sensitivities are not ideal, and prior discussions have largely been confined to camera-specific color spaces, making it difficult to achieve physically accurate radiometric compensation. In contrast, by using a 2DSR, it becomes possible to acquire spectrally resolved, physically grounded measurements, enabling spectral-level radiometric compensation and compensation that minimizes color differences in arbitrary color spaces. In particular, by making color spaces based on human visual characteristics differentiable with respect to spectral data, we achieved radiometric compensation that accounts for human color perception. The experimental results using a physical prototype in Sec. 3 show that the proposed method achieves more accurate projector radiometric compensation that better aligns with human color perception than conventional methods using an RGB camera [15,18]. On the other hand, the proposed method has the following limitations.

First, the proposed method cannot be directly applied when the target spectral image and the captured spectral image have different numbers of spectral bands. In our formulation, the objective functions compute the difference between the target and captured spectral data, which requires both spectral data to have the same number of bands. To handle spectral images with different band counts, one straightforward approach is to upsample the spectral data with fewer bands; however, this may only introduce unnecessary redundancy and waste computational resources. A more promising approach is to downsample the projection function or the captured spectral image to match the band count of the target spectral image. Fubara et al. [35] reported that spectra of natural scenes often lie in a low-dimensional subspace and can be approximated by around ten basis functions. In addition, since typical RGB projectors represent colors using a limited number of primaries (e.g., three or six), the projector spectral power distributions are also expected to lie in a low-dimensional subspace. Therefore, by representing the projection function and/or the captured spectral data using basis functions and downsampling them to match the target band count, it should become possible to handle spectral images with different numbers of bands. This direction is expected not only to enable support for different band counts, but also to substantially reduce measurement and computational costs. At the same time, however, we do not claim that a reduced spectral representation necessarily provides compensation performance comparable to that of the full 401-band representation, because, in practical environments, reducing the spectral dimensionality may increase the influence of ambient illumination, sensor noise, model inaccuracy, and the interaction between the projector spectra and the object reflectance spectra. Investigating the trade-off between spectral dimensionality, compensation accuracy, and computational efficiency remains an important direction for future work.

Second, the proposed method has limited flexibility to changes in the setup. As with other radiometric compensation methods that assume a static setup, our method models the projector spectral characteristics and the spectral reflectance of the projection surface jointly as a projection function; therefore, when the setup changes, the projection function must be re-estimated. Moreover, because we model each projector pixel independently (i.e., without sharing information across pixels), the calibration is data-inefficient. Consequently, achieving high-accuracy radiometric compensation over the entire projection surface requires collecting spectral measurements for many known RGB inputs separately at each pixel. However, since the projector spectral distributions should be spatially almost uniform, we expect that separating the estimation of the surface reflectance from the projector spectral characteristics could reduce the number of captured spectral images required for estimating the parameters of the projector-2DSR color transformation model. For RGB-camera-based methods, there are studies that attempt to separately estimate the projector spectral characteristics and the surface reflectance [19], but due to metamerism, information about surface reflectance and spectral distributions is incomplete, making the estimation relatively difficult and providing no guarantee of physical correctness. In contrast, using a 2DSR may enable physically accurate estimation by separating

Optics EXPRESS

these characteristics. Compared with RGB-camera-based methods, the proposed 2DSR-based framework involves clear practical trade-offs. RGB cameras are more accessible and allow faster acquisition, making them more suitable for dynamic or real-time projection mapping scenarios. In contrast, a 2DSR provides spectrally resolved and physically grounded measurements, enabling more accurate radiometric compensation and optimization in spectral and perceptually motivated color spaces, but at the cost of slower acquisition. Therefore, the present implementation is better suited to applications such as product design, in which high-fidelity color reproduction is prioritized over speed.

5. Conclusion

In this paper, we proposed a projector radiometric compensation method with high-fidelity color reproduction using a 2DSR. To perform radiometric compensation using spectral data, we formulated the projection process with a spectral-level model and proposed an optimization method that minimizes spectral error as well as color differences in differentiable color spaces. By estimating the projection function in the spectral domain, our method enables explicit minimization of spectral error between the target image and the projected result, which was not possible with conventional approaches. Experimental results with a physical prototype demonstrate that the proposed method achieves more accurate projector radiometric compensation that better aligns with human color perception than conventional methods using an RGB camera.

As future work, we plan to extend our framework by incorporating a multiband projector or a hyperspectral projector, aiming at full reproduction of the desired spectral radiance. In addition, we will investigate acceleration strategies, including reducing the computational cost of spectral-image-based optimization through spectral dimensionality reduction and enabling faster processing via one-shot estimation. We will also investigate ways to improve the practical usability of the proposed framework as hyperspectral imaging hardware becomes faster and more accessible.

Funding. Japan Society for the Promotion of Science (JP25K22820).

Acknowledgments. The authors thank Prof. Kowa Koida for insightful comments on color science and terminology.

Disclosures. The authors declare no conflicts of interest.

Data availability. Data underlying the results presented in this paper are not publicly available at this time but may be obtained from the authors upon reasonable request.

References

1. M. R. Mine, J. Van Baar, A. Grundhöfer, *et al.*, "Projection-based augmented reality in Disney theme parks," Computer **45**(7), 32–40 (2012).
2. B. R. Jones, H. Benko, E. Ofek, *et al.*, "IllumiRoom," in *Proceedings of the SIGCHI Conference on Human Factors in Computing Systems*, (2013), pp. 869–878.
3. B. Jones, R. Sodhi, M. Murdock, *et al.*, "RoomAlive," in *Proceedings of the 27th Annual ACM Symposium on User Interface Software and Technology*, (2014), pp. 637–644.
4. H. Nishino, E. Hatano, S. Seo, *et al.*, "Real-time navigation for liver surgery using projection mapping with indocyanine green fluorescence: development of the novel medical imaging projection system," Ann. Surg. **267**(6), 1134–1140 (2018).
5. A. H. Bermano, M. Billeter, D. Iwai, *et al.*, "Makeup lamps: live augmentation of human faces via projection," Computer Graphics Forum **36**(2), 311–323 (2017).
6. C. Siegl, V. Lange, M. Stamminger, *et al.*, "FaceForge: markerless non-rigid face multi-projection mapping," IEEE Trans. Visual. Comput. Graphics **23**(11), 2440–2446 (2017).
7. M. R. Marner, R. T. Smith, J. A. Walsh, *et al.*, "Spatial user interfaces for large-scale projector-based augmented reality," IEEE Comput. Grap. Appl. **34**(6), 74–82 (2014).
8. H. Zhang, P. Chen, J. Yang, *et al.*, "IEDS: exploring an intelli-embodied design space combining designer, AR, and GAI to support industrial conceptual design," in *Proceedings of the 2025 CHI Conference on Human Factors in Computing Systems*, pp. 1–25 (2025).
9. C. Menk, E. Jundt, and R. Koch, "Visualisation techniques for using spatial augmented reality in the design process of a car," Computer Graphics Forum **30**(8), 2354–2366 (2011).

Optics EXPRESS

10. R. Raskar, P. Beardsley, J. Van Baar, *et al.*, "RFIG lamps: interacting with a self-describing world via photosensing wireless tags and projectors," ACM Trans. Graph. **23**(3), 406–415 (2004).
11. K. Matsushita, D. Iwai, and K. Sato, "Interactive bookshelf surface for in situ book searching and storing support," *ACM International Conference Proceeding Series* (2011).
12. Y. Kitajima, D. Iwai, and K. Sato, "Simultaneous projection and positioning of laser projector pixels," IEEE Trans. Visual. Comput. Graphics **23**(11), 2419–2429 (2017).
13. D. Iwai and K. Sato, "Document search support by making physical documents transparent in projection-based mixed reality," Virtual Reality **15**(2-3), 147–160 (2010).
14. S. K. Nayar, H. Peri, M. D. Grossberg, *et al.*, "A projection system with radiometric compensation for screen imperfections," in *ICCV Workshop on Projector-Camera Systems (PROCAMS)*, vol. 3 (2003), p. 1.
15. T. Yoshida, C. Horii, and K. Sato, "A virtual color reconstruction system for real heritage with light projection," *Proceedings of VSMM* (2003).
16. A. Grundhofer and D. Iwai, "Robust, error-tolerant photometric projector compensation," IEEE Transactions on Image Processing **24**(12), 5086–5099 (2015).
17. B. Huang and H. Ling, "End-to-end projector photometric compensation," in *2019 IEEE/CVF Conference on Computer Vision and Pattern Recognition (CVPR)*, vol. 2019-June (2019), pp. 6803–6812.
18. B. Huang, T. Sun, and H. Ling, "End-to-end full projector compensation," IEEE Trans. Pattern Anal. Mach. Intell. **44**(6), 2953–2967 (2022).
19. Y. Li, W. Yin, J. Li, *et al.*, "Physics-based efficient full projector compensation using only natural images," IEEE Trans. Visual. Comput. Graphics **30**(8), 4968–4982 (2024).
20. J. Park, D. Jung, and B. Moon, "Projector compensation framework using differentiable rendering," IEEE Access **10**, 44461–44470 (2022).
21. Y. Kageyama, M. Isogawa, D. Iwai, *et al.*, "ProDebNet: projector deblurring using a convolutional neural network," Opt. Express **28**(14), 20391 (2020).
22. B. Huang and H. Ling, "DeProCams: simultaneous relighting, compensation and shape reconstruction for projector-camera systems," IEEE Trans. Visual. Comput. Graphics **27**(5), 2725–2735 (2021).
23. Y. Kageyama, D. Iwai, and K. Sato, "Efficient distortion-free neural projector deblurring in dynamic projection mapping," IEEE Trans. Visual. Comput. Graphics **30**(12), 7544–7557 (2024).
24. G. D. Finlayson, M. Mackiewicz, and A. Hurlbert, "Color correction using root-polynomial regression," IEEE Trans. on Image Process. **24**(5), 1460–1470 (2015).
25. G. D. Finlayson and Y. Zhu, "Designing color filters that make cameras more colorimetric," IEEE Trans. on Image Process. **30**, 853–867 (2021).
26. R. Von Luther, "Aus dem gebiet der farbreizmetrik," Zeitschrift fur technishe physik **12**, 540–558 (1927).
27. H. E. Ives, "The transformation of color mixture equations from one system to another. II. Graphical aids," J. Franklin Inst. **195**(1), 23–44 (1923).
28. J. Zhang, K. A. G. Smet, and Y. Meuret, "Tuning color and saving energy with spatially variable laser illumination," Opt. Express **27**(19), 27136–27150 (2019).
29. G. Wyszecki and W. S. Stiles, Color Science (2000).
30. K. Sato and S. Inokuchi, "Liquid crystal range finder—a high-speed range-imaging system using liquid crystal shutter," Systems and Computers in Japan **20**(8), 89–99 (1989).
31. CIE, "CIE 1931 colour-matching functions, 2 degree observer," Tech. rep., International Commission on Illumination (2019).
32. S. Süsstrunk, R. Buckley, and S. Swen, "Standard RGB color spaces," Color and Imaging Conference **7**(1), 127–134 (1999).
33. I. Kauvar, S. J. Yang, L. Shi, *et al.*, "Adaptive color display via perceptually-driven factored spectral projection," ACM Trans. Graph. **34**(6), 1–10 (2015).
34. D. C. Liu and J. Nocedal, "On the limited memory BFGS method for large scale optimization," Mathematical Programming **45**(1-3), 503–528 (1989).
35. B. J. Fubara, M. Sedky, and D. Dyke, "RGB to spectral reconstruction via learned basis functions and weights," in *Proceedings of the IEEE/CVF Conference on Computer Vision and Pattern Recognition Workshops*, (2020), pp. 480–481.